Communication

Enantioselective Hydroxylation of Benzylic C(sp3)-H Bonds by an Artificial Iron Hydroxylase Based on the Biotin-Streptavidin Technology

Joan Serrano-Plana, Corentin Rumo, Johannes G. Rebelein, Ryan Loren Peterson, Maxime Barnet, and Thomas R. Ward

J. Am. Chem. Soc., **Just Accepted Manuscript** • DOI: 10.1021/jacs.0c02788 • Publication Date (Web): 26 May 2020

a)

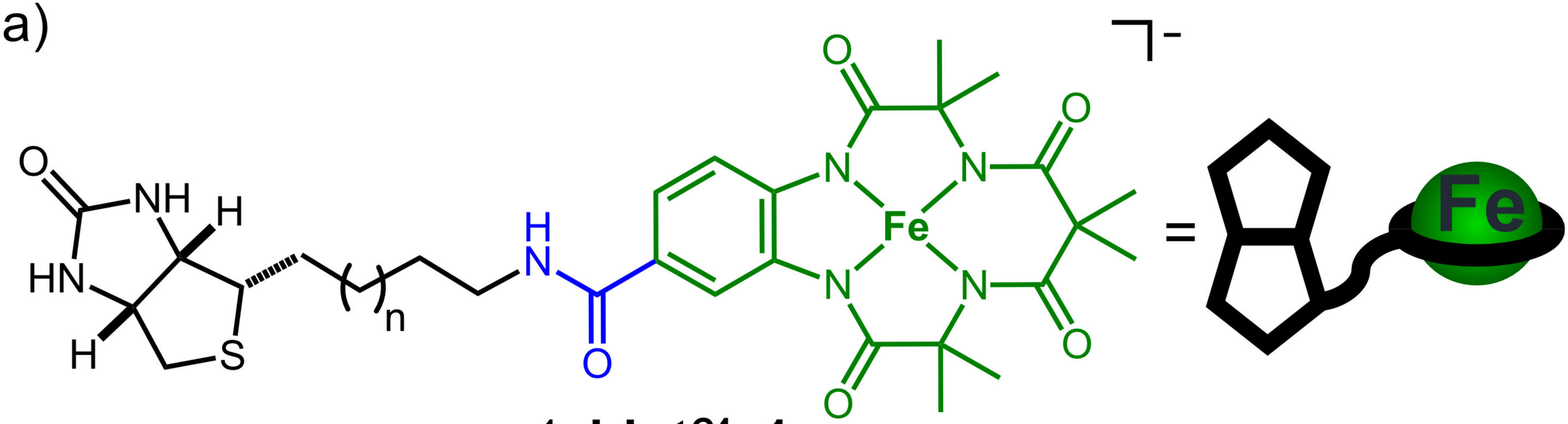

n = 1 **biot^{C4}–1**

n = 2 **biot^{C5}–1**

b)

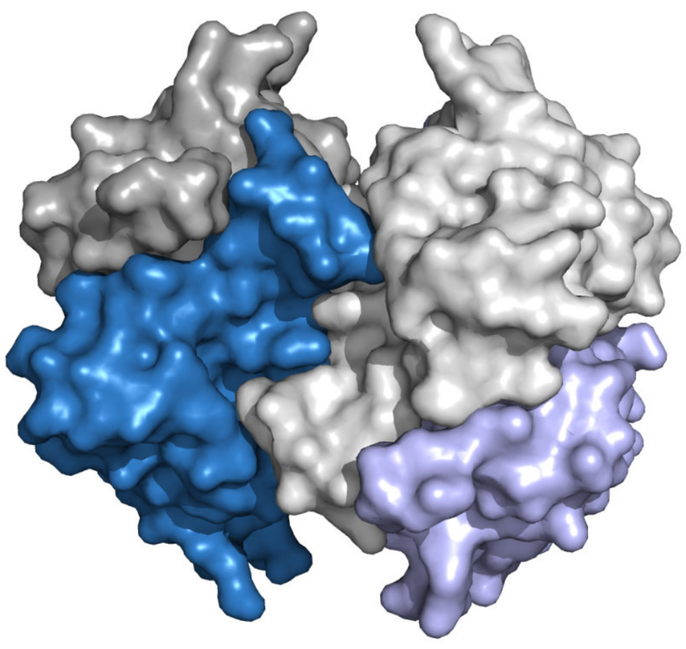

Streptavidin (Sav)

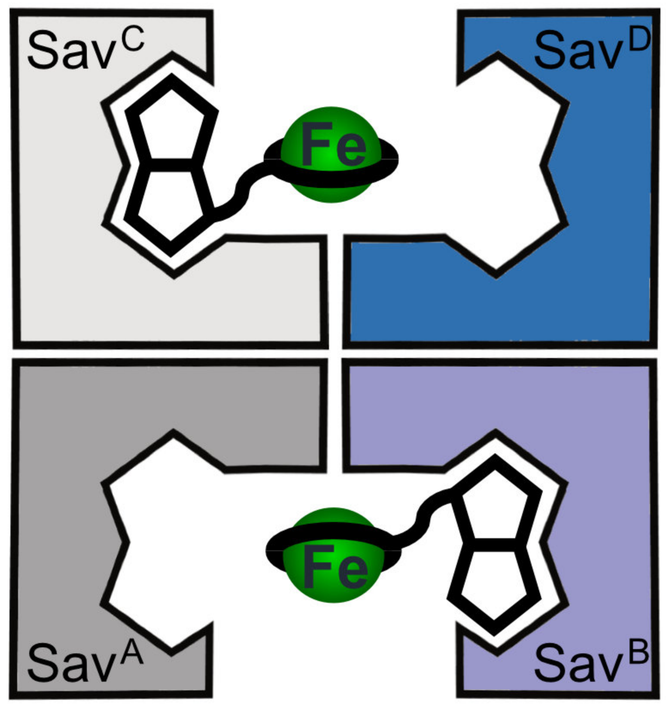

biot^{Cn}–1 · Sav

artificial hydroxylase

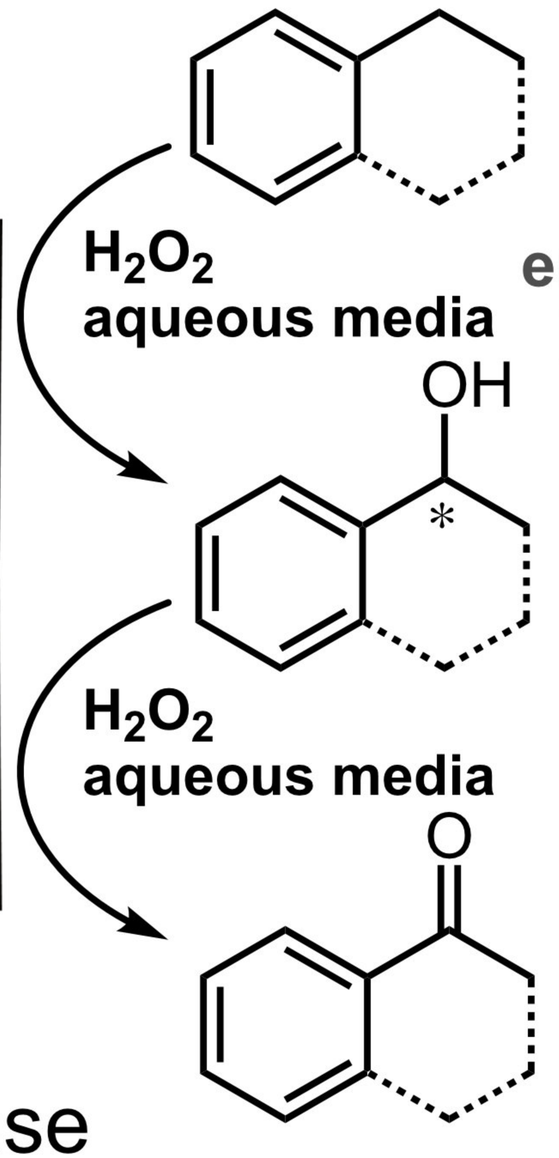

enantioselective hydroxylation

kinetic resolution

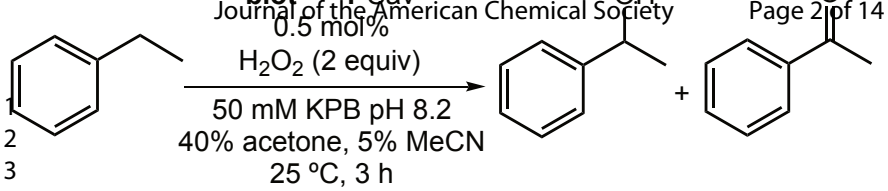

Sav variant	Cofactor biotCn–1 C4	C5
No Sav		
WT		
S112A		
S112L		
S112M		
S112F		
S112Y		
S112W		
S112T		
S112Q		
S112R		
S112H		
S112K		
S112E		
S112C		
S112P		

Sav variant	Cofactor biotCn–1 C4	C5
S112G		
K121A		
K121V		
K121I		
K121M		
K121F		
K121W		
K121S		
K121P		
K121R		
K121H		
K121D		
K121C		
S112A/K121L		
S112Y/K121R		
S112R/K121E		

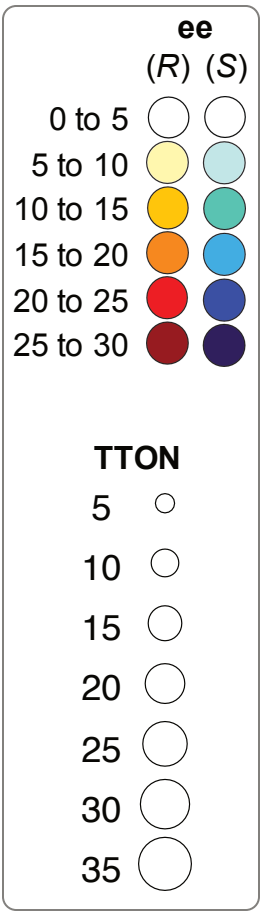

a)

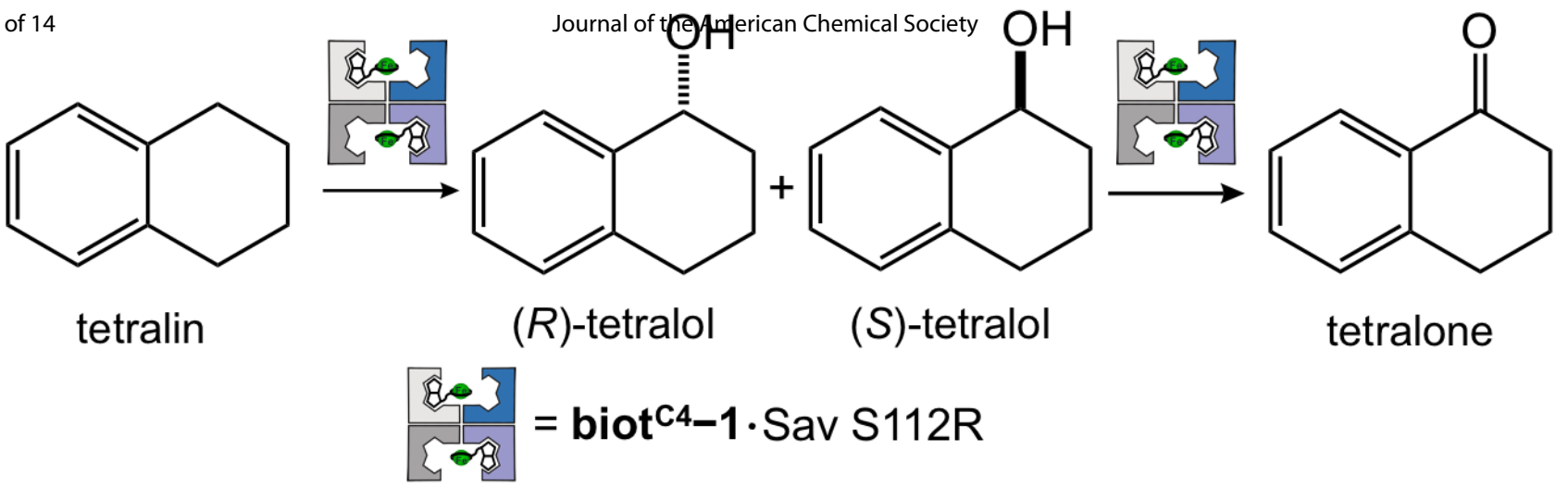

b)

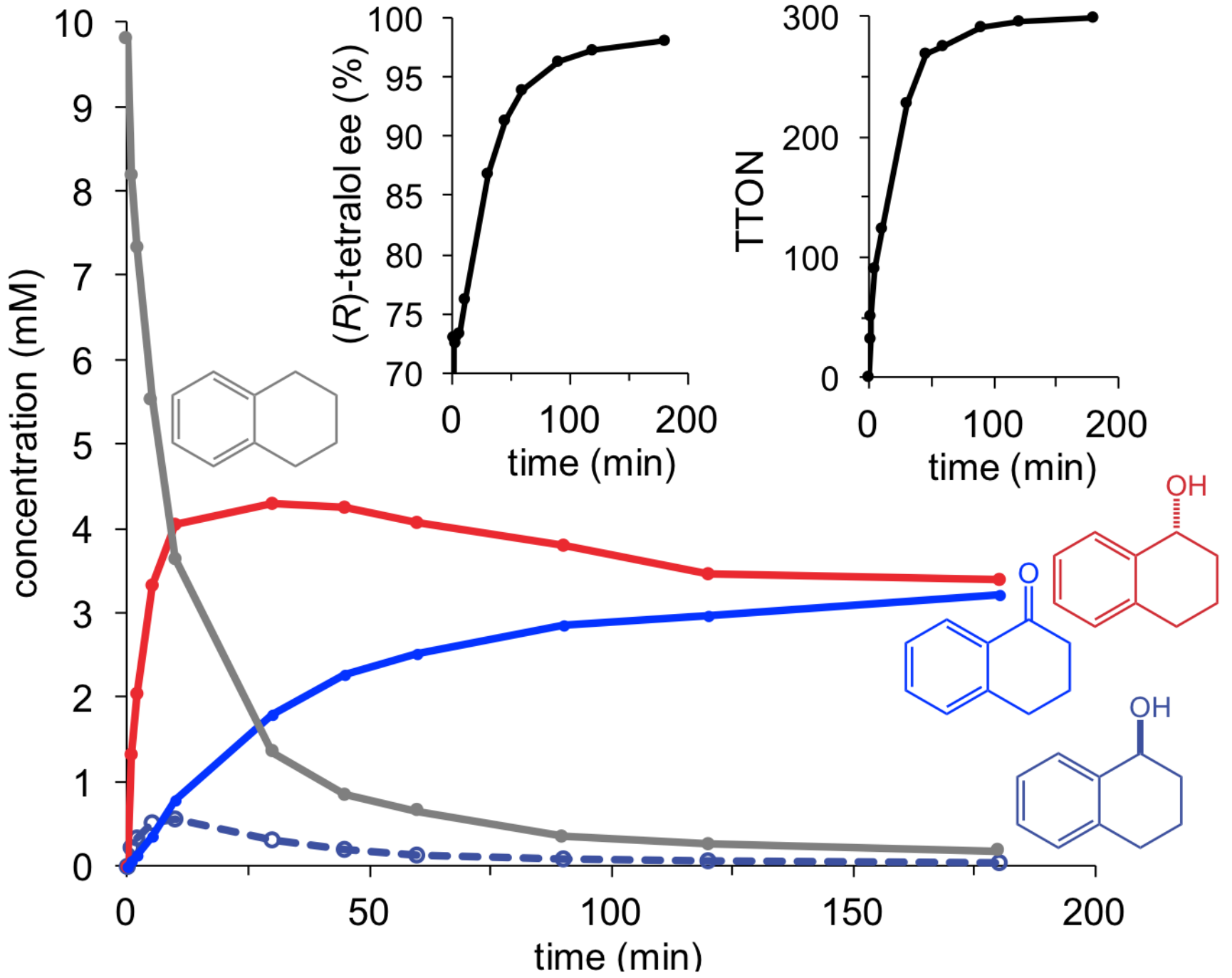

c)

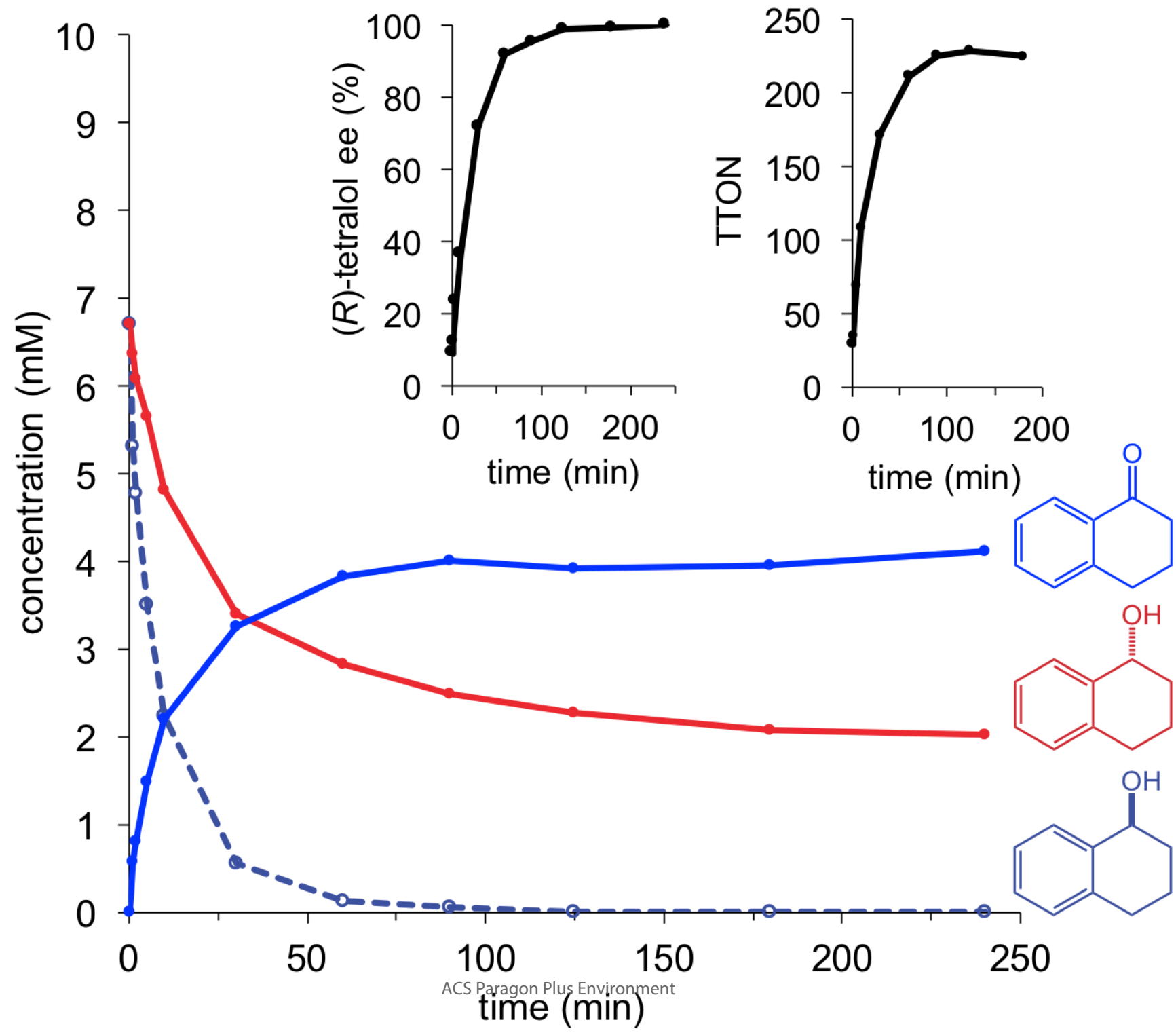

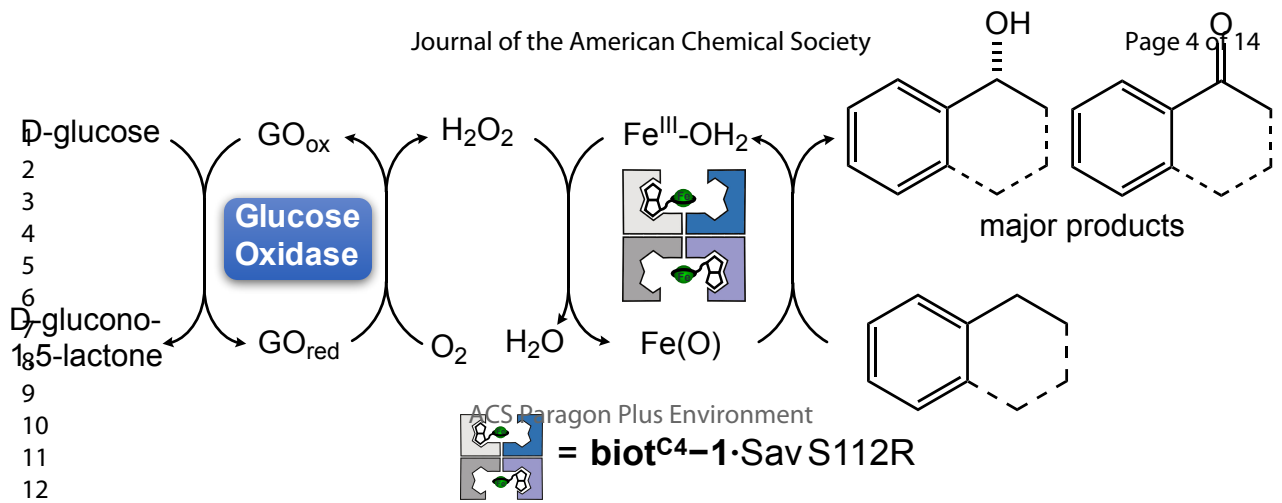

a)

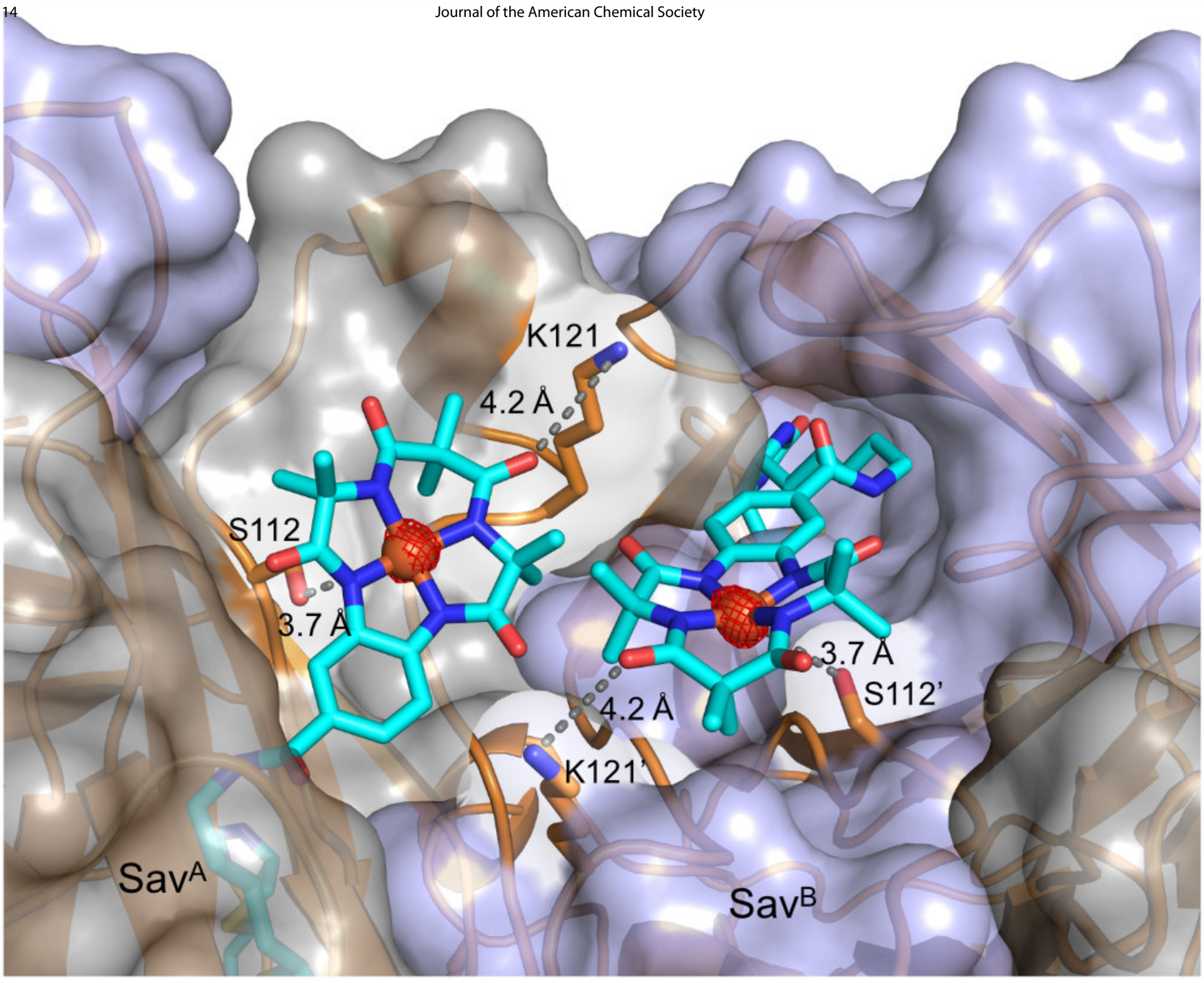

b)

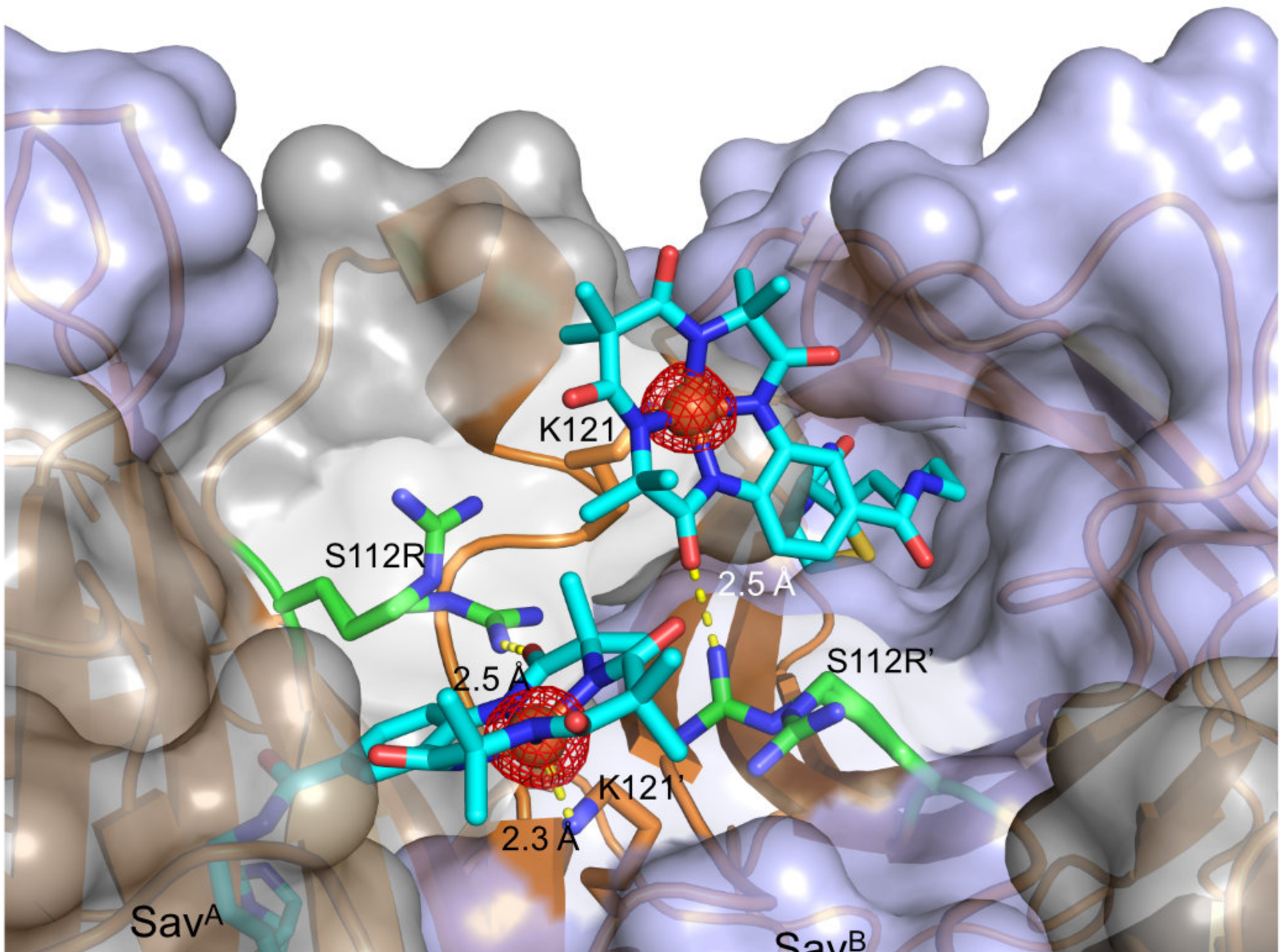

c)

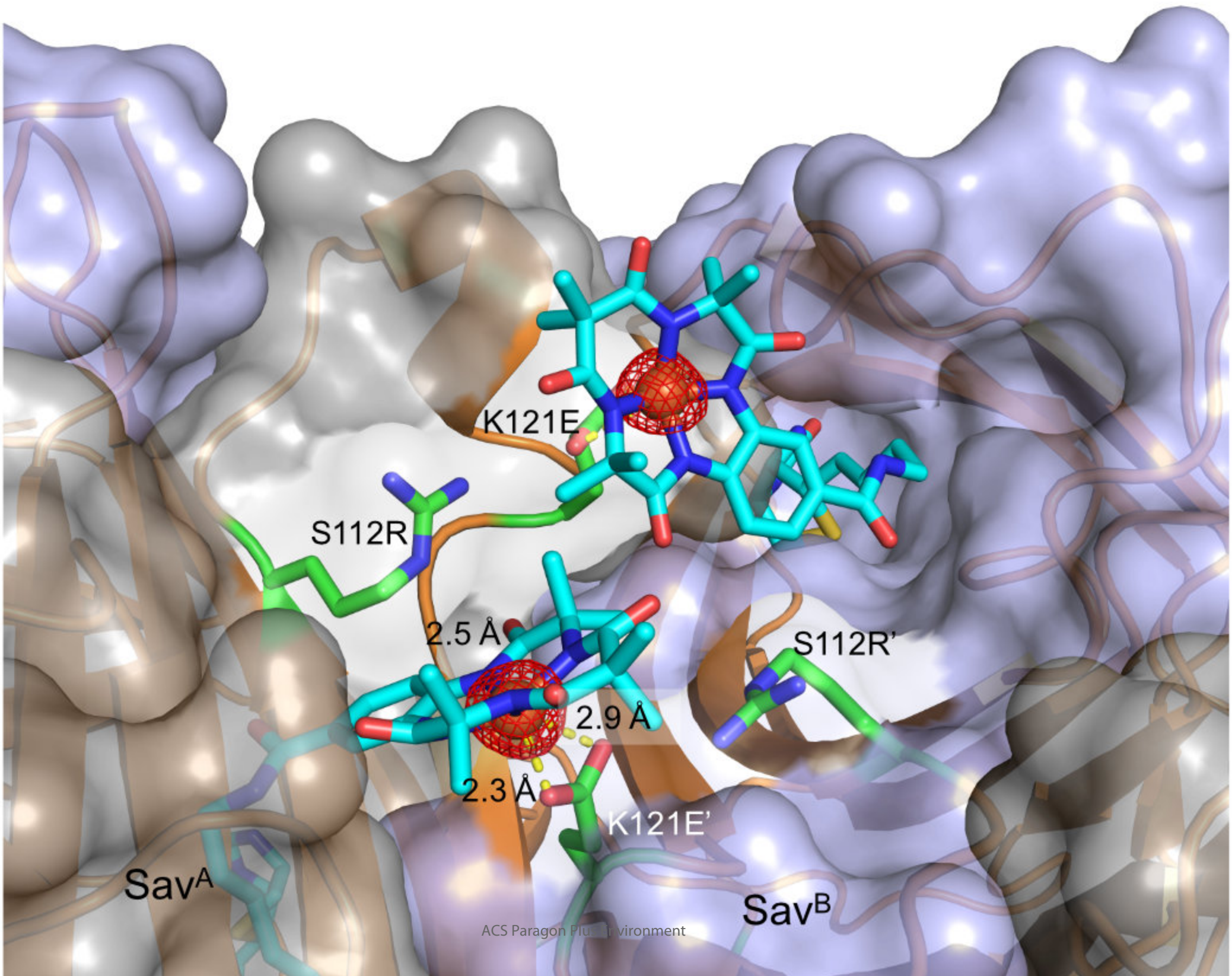

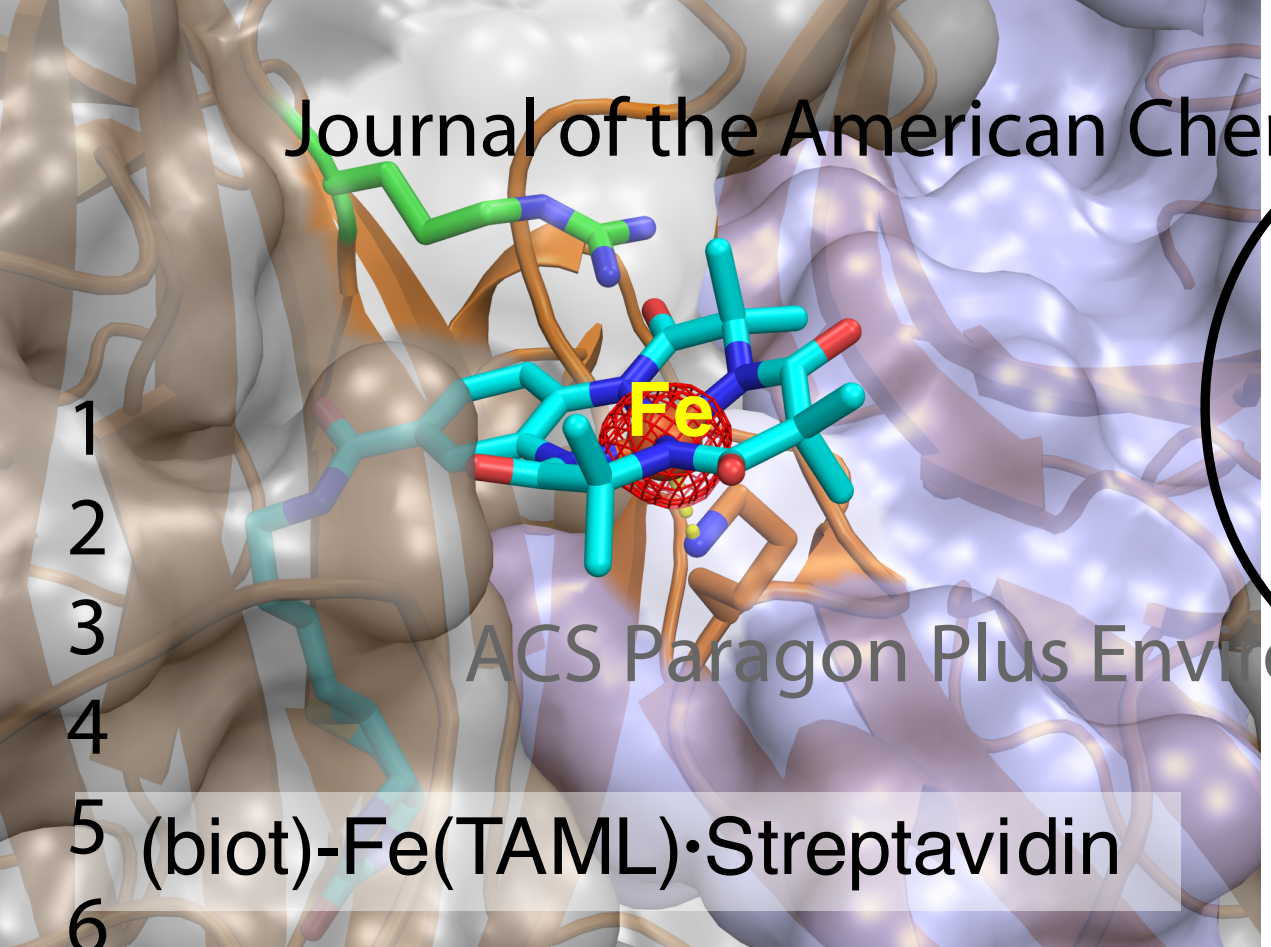

(biot)-Fe(TAML)·Streptavidin

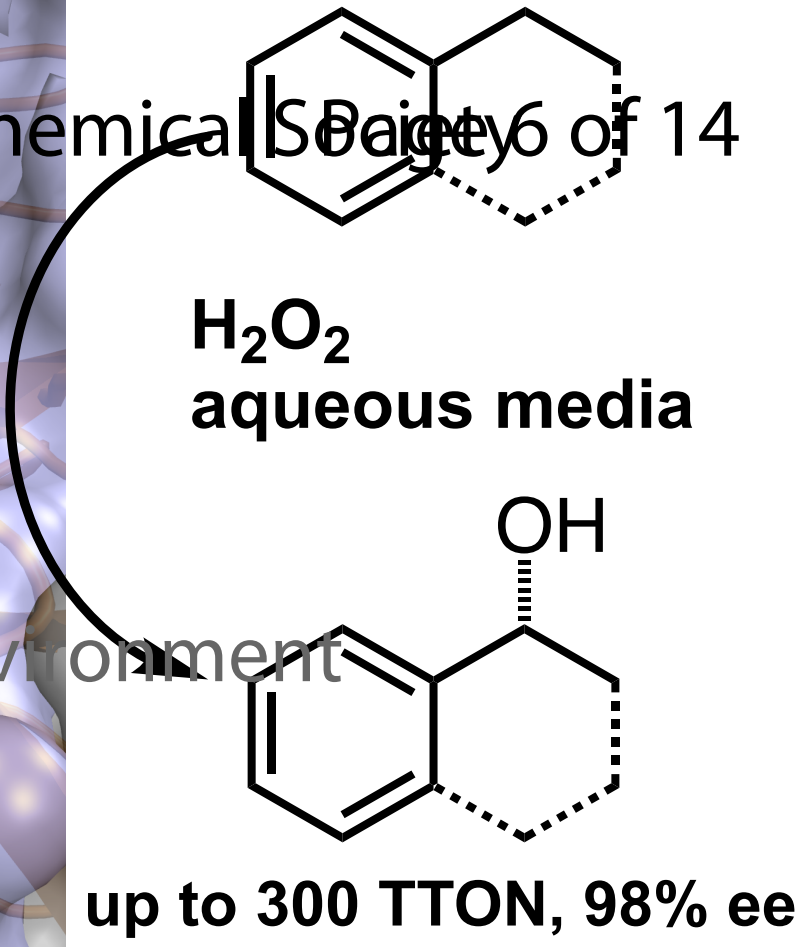

Substrate		TTON	ee (%)	[alcohol]/[ketone]	Conversion (%) (alcohol yield (%))[c]
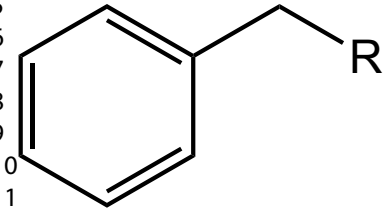	R = CH_3	57	32	3.2	11.5 (8.8)
	R = CH_2CH_3	26	45	8.4	5.9 (5.3)
	R = $(CH_2)_2CH_3$	19	45	7.5	4.3 (3.8)
	R = $C(CH_3)_2$	0	-	-	-
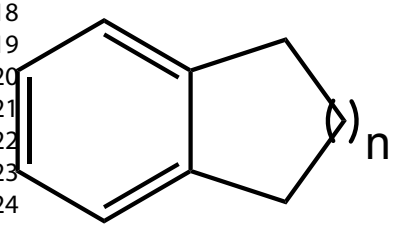	n = 2	316	65	5.7	60 (44.3)
		300[b]	>98	1.1	86.8 (34.3)
	n = 1	205	47	7.4	45.7 (40.2)
		173[b]	80	0.8	55.7 (24.7)
	n = 0	0	-	-	-
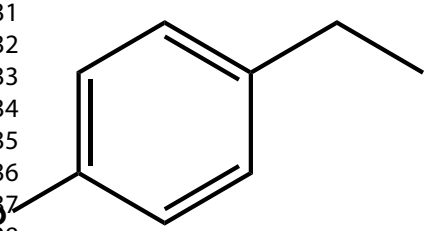	R = OCH_3	120	12	5.9	26.3 (22.5)
	R = Cl	20	14	3.8	4.1 (3.3)
	R = Br	9	18	>20	2.3 (2.3)

Enantioselective Hydroxylation of Benzylic C(sp^3)-H Bonds by an Artificial Iron Hydroxylase Based on the Biotin-Streptavidin Technology

Joan Serrano-Plana, Corentin Rumo, Johannes G. Rebelein, Ryan L. Peterson, Maxime Barnet, Thomas R. Ward*

Department of Chemistry, University of Basel, BPR1096, Mattenstrasse 24a, CH-4058 Basel Switzerland

Supporting Information Placeholder

ABSTRACT: The selective hydroxylation of C–H bonds is of great interest to the synthetic community. Both homogenous catalysts and enzymes offer complementary means to tackle this challenge. Herein, we show that biotinylated Fe(TAML)-complexes (TAML = Tetra Amido Macrocyclic Ligand) can be used as cofactors for incorporation into streptavidin to assemble artificial hydroxylases. Chemo-genetic optimization of both cofactor and streptavidin allowed optimizing the performance of the hydroxylase. Using H_2O_2 as oxidant, up to ~300 turnovers for the oxidation of benzylic C–H bonds were obtained. Upgrading the ee was achieved by kinetic resolution of the resulting benzylic alcohol to afford up to >98% ee for (*R*)-tetralol. X-ray analysis of artificial hydroxylases highlights critical details of the second coordination sphere around the Fe(TAML) cofactor.

The selective functionalization of C–H bonds represents one of the frontiers in synthetic methodology.[1-7] To address this challenge, homogeneous catalysis often relies on directing groups present on the substrate that coordinate to the metal center, thus allowing distinguishing between equally reactive C–H bonds.[7] Enzymes have been optimized thanks to evolution to differentiate C–H bonds with exquisite selectivity: The active site around the cofactor is tailored to ensure proper orientation of the substrate.

For the hydroxylation of inert C–H bonds, iron-containing enzymes and iron-based homogeneous catalysts occupy a place of choice. They are complementary in many respects. While the former operate under physiological conditions, homogeneous catalysts perform best at low temperature in organic solvents. The reactivity of homogeneous catalysts is often tuned via first-coordination sphere modifications, whereas enzymes rely on secondary sphere interactions.

Iron metalloenzymes catalyze the C–H oxyfunctionalization of hydrocarbons *via* iron-oxygen species resulting from activation of O_2.[8-17] The selective hydroxylation of C–H bonds using homogeneous catalysts has been achieved by designing structurally-elaborated ligands that provide a tailored cavity around the metal center.[18-33]

To complement homogeneous catalysts and enzymes, artificial metalloenzymes (ArMs), that result from anchoring an abiotic cofactor within a macromolecular scaffold, have attracted increasing interest in the past years. The well-defined secondary coordination sphere around the cofactor provided by the protein offers fascinating perspectives to optimize both activity and selectivity of the ArMs.[34-39] In this context several protein scaffolds have proven versatile.[34] These include carbonic anhydrase,[40] hemoproteins,[41-42] proline oligopeptidase,[43] lactococcal multiresistance regulator,[44] four helix bundles,[45-46] nitrobindin,[47] (strept)avidin,[48-50] etc. In the context of asymmetric C–H hydroxylation, introduction of an Mn-porphycene cofactor within myoglobin afforded promising ArMs[51] that complement evolved cytochrome P450 enzymes.[52-54]

Fe(TAML) complexes are a versatile family of iron complexes that typically contain a ferric center tightly bound to a tetraamido macrocyclic ligand.[55-56] Their reactivity as peroxidase mimics has been extensively studied.[55,57-58] Some Fe(TAML) complexes hydroxylate hydrocarbons in aqueous media using oxidants such as *t*BuOOH or *m*-CPBA[56,59-61] or electrochemically.[62] Thanks to their stability in water, we surmised that Fe(TAML) complexes may allow to assemble an iron-based artificial hydroxylase using the biotin-streptavidin technology. The secondary coordination sphere provided by streptavidin (Sav), may enable enantioselective hydroxylation and minimize the formation of less reactive dimeric species.

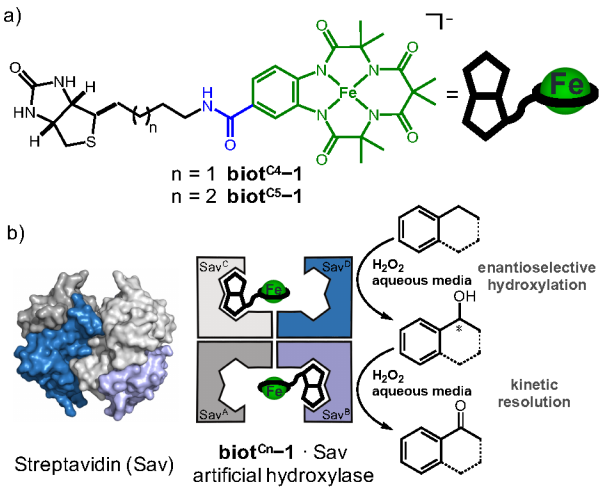

Scheme 1. Artificial C–H hydroxylase based on biotin-streptavidin. a) Structure of cofactors **biot^{C4}–1** and **biot^{C5}–1**. To increase the electron-withdrawing property of the ligand, a biotin amine was coupled to Fe-TAML (green) bearing a carboxylic acid to afford an "inverted" amide (blue); b) representation of the ArM resulting from anchoring **biot^{Cn}–1** in streptavidin.

Initial ligand design and reactivity tests. Sav is a homotetrameric protein that displays exceptional affinity for biotinylated probes (K_d 10^{-14} M) and maintains its function and quaternary structure in the presence of various chaotropic agents (pH, temperature, cosolvent tolerance, etc.).[48,50,63] To ensure localization of the TAML cofactor within Sav, we synthesized a complex bearing a biotin anchor, **biot^{C5}–1**. It was designed to bind to the Fe-TAML moiety through an "inverted" amide bond to the aromatic ring (Scheme 1a) to increase the electron withdrawing effect, which has been shown to be beneficial for the reactivity of Fe-TAML complexes.[64]

Initial reactivity tests were performed with ethylbenzene (PhEt, $BDE_{C\text{-}H}$ = 87 kcal/mol) using 2 equiv. H_2O_2 in phosphate buffer (KPB) at pH 8.2 and 40% acetone for 3 h.[61,65] Under these conditions, **biot^{C5}–1**·Sav WT afforded (*rac*)-1-phenylethanol ((*rac*)-PhEtOH)) and acetophenone (23 total turnover number, TTON[66]). Both activity and selectivity of **biot^{C5}–1**·Sav WT were comparable to the free cofactor **biot^{C5}–1** (21 TTON, (*rac*)-PhEtOH). Next, we screened a Sav library that included mutations at positions Sav S112X and/or Sav K121X (Scheme 2 and Table S4). The TTON and enantioselectivity remained modest (up to 16% ee (*R*)-PhEtOH and 29 TTON). We hypothesized that the moderate influence of the host protein on the catalytic performance may be due to the poor localization of the Fe-TAML within the biotin-binding vestibule. We surmised that a shorter biotin **C^n**-linker may increase the influence of Sav on the catalytic performance by positioning the metal center deeper within the binding pocket. We prepared **biot^{C4}–1** and evaluated its performance (Scheme 1, 2 and Table S4).

Shortening the **C^n**-linker positively affects the selectivity: **biot^{C4}–1**·Sav WT affords 6% ee (*R*)-PhEtOH. Screening the above Sav library with **biot^{C4}–1** reveals that close-lying aminoacids influence the ee: **biot^{C4}–1**·Sav S112R yields 28% ee (*R*)-PhEtOH (28 TTON), and **biot^{C4}–1**·Sav S112R/K121E affords 24% ee (*S*)-PhEtOH (29 TTON).

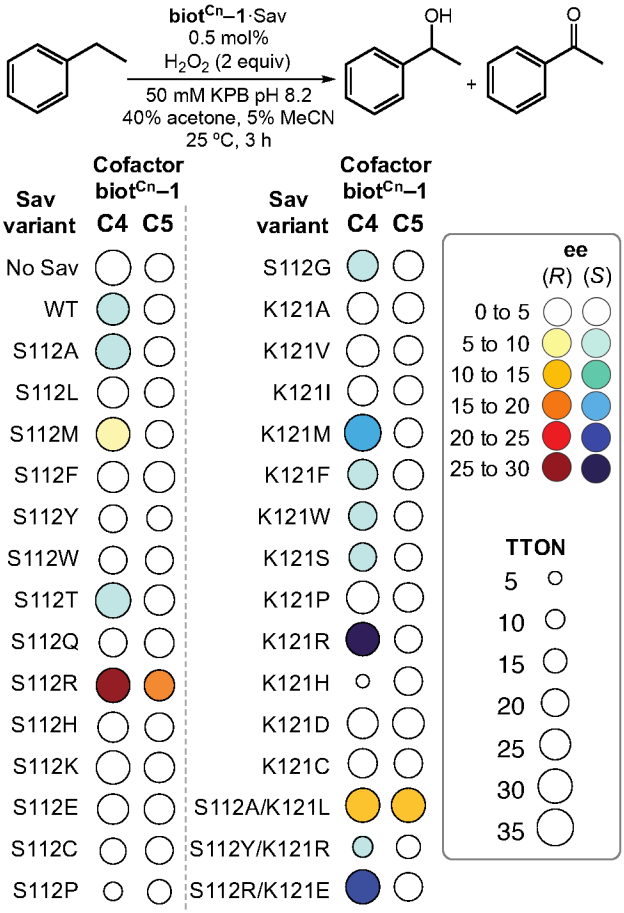

Scheme 2. Fingerprint summary of the artificial hydroxylase optimization with PhEt.

Intrigued by these findings, the oxidation of PhEt by **biot^{C4}–1**·Sav S112R was monitored. Two consecutive oxidation steps take place. Initially, hydroxylation of the benzylic position affords (*R*)-PhEtOH with ee > 40% after a few TTON (Figure S8). As the reaction progresses, the formation of acetophenone is observed along with a gradual erosion of the ee. This suggests that the alcohol oxidation is (partially) stereospecific: (*R*)-PhEtOH is oxidized preferentially to acetophenone. Indeed, kinetic resolution of (*rac*)-PhEtOH by **biot^{C4}–1**·Sav S112R affords acetophenone (38 TTON), leaving enantioenriched (*S*)-PhEt (20% ee after 3 hours, $E = k_{(R)}/k_{(S)} = 3.4$, Figure S9).

In contrast, product analysis after PhEt oxidation by **biot^{C4}–1**·Sav (Sav: K121R or S112R/K121E) yielded ee of (*S*)-PhEtOH (Scheme 2), the opposite enantiomer than **biot^{C4}–1**·Sav S112R. However, monitoring product formation over time reveals a similar reaction pathway for all three ArMs: The hydroxylation of PhEt yields preferentially (*R*)-PhEtOH, which is then oxidized faster to acetophenone (Figure S10-11). This mechanistic pathway is reflected in an erosion of ee over time, eventually affording (*S*)-PhEtOH with both Sav K121R and Sav S112R/K121E. Indeed, the ee is highly variable, depending on conversion and mutant.

The reaction conditions to improve performance of the hydroxylase were fine-tuned for **biot^{C4}–1**·Sav S112R. A large excess of H_2O_2 favors overoxidation and erosion of ee (Figure S13). The impact of Sav on the activity is also evident at different pHs: **biot^{C4}–1**·Sav S112R displays maximum TTON and enantioselectivity at 8.2 < pH < 8.8. Outside this widow, the activity decreases markedly (Figure S14). The free cofactor **biot^{C4}–1** has maximum activity at 6 < pH < 8 and is quenched at higher pH.

Structural Characterization. To scrutinize the differences in the second coordination sphere that influence the activity of the ArMs, we determined their structure by crystallography. Data sets were obtained for **biot^{C4}–1**·Sav and **biot^{C5}–1**·Sav (Sav = WT, S112R, and S112R/K121E, Table S1 and S2).

The structures reveal the following features: all six structures are nearly superimposable, reflected by a C_α–RMSD varying between 0.038–0.256 Å (Table S3). The electron density of the Fe-TAML moiety is defined for **biot^{C4}–1**, the Fe-occupancy is 60% for Sav WT and 100% for Sav S112R and S112R/K121E (Figure 1). This contrasts with **biot^{C5}–1**, for which only the electron density of the biotin C_5–linker is defined and modelled with 100% occupancy (Figure S5-S7). We tentatively trace this to the higher flexibility of the C_5-linker, resulting in delocalization of the Fe-TAML moiety.

The localization of the Fe(TAML) moiety is affected by the residue at position 112 (Figure 1 and S2-S4). For **biot^{C4}–1**·Sav WT, the closest amino acids are Sav^A S112 (3.7 Å) and Sav^B K121' (4.2 Å). They hardly interact with Fe(TAML), resulting in a reduced occupancy of Fe(TAML). The mutation Sav S112R forces the Fe(TAML) into a fixed conformation with 100% occupancy, placing the arginine within H-bonding distance to the C=O of the Fe(TAML) (2.5 Å, in one of two conformations, Figure 1b). This alternative position of Fe(TAML) allows Sav^B K121' to coordinate to Fe of **biot^{C4}–1**·Sav^A (2.3 Å, Figure 1b). To enable the coordination of Sav^B K121' to the Fe of **biot^{C4}-1**, the lysine side-chain adopts a compact conformation with acute dihedral (χ) angles of 54.2°, 106.9°, 80.0° and 41.2°. We hypothesize that both the precise localization of the Fe(TAML) and its interaction with either K121' or E121' through an η^2-coordination (in **biot^{C4}–1**·Sav S112R/K121E, Fe···O 2.3 and 2.9 Å, Figure 1c) impact the catalysis outcome (product distribution and ee, Scheme 2).

Substrate scope. The substrate scope for **biot^{C4}–1**·Sav S112R was expanded to substrates containing benzylic C_{sp^3}–H bonds (Table 1). Propylbenzene and butylbenzene afforded the corresponding (*R*)-alcohol in 45% ee (26 and 19 TTON, respectively). Electron-rich *p*-substituted ethylbenzenes afforded higher TTONs, highlighting the electrophilic character of the Fe(O) species (Figure S15).

A kinetic isotope effect KIE = 9.2 was determined for the oxidation of PhEt/PhEt-d_{10} by **biot^{C4}–1**·Sav S112R at 25 ºC (Figure S16). This value compares well with previously described KIE for Fe-TAML complexes and suggests that the rate determining step of the reaction is the hydrogen abstraction.[56,60,67-68]

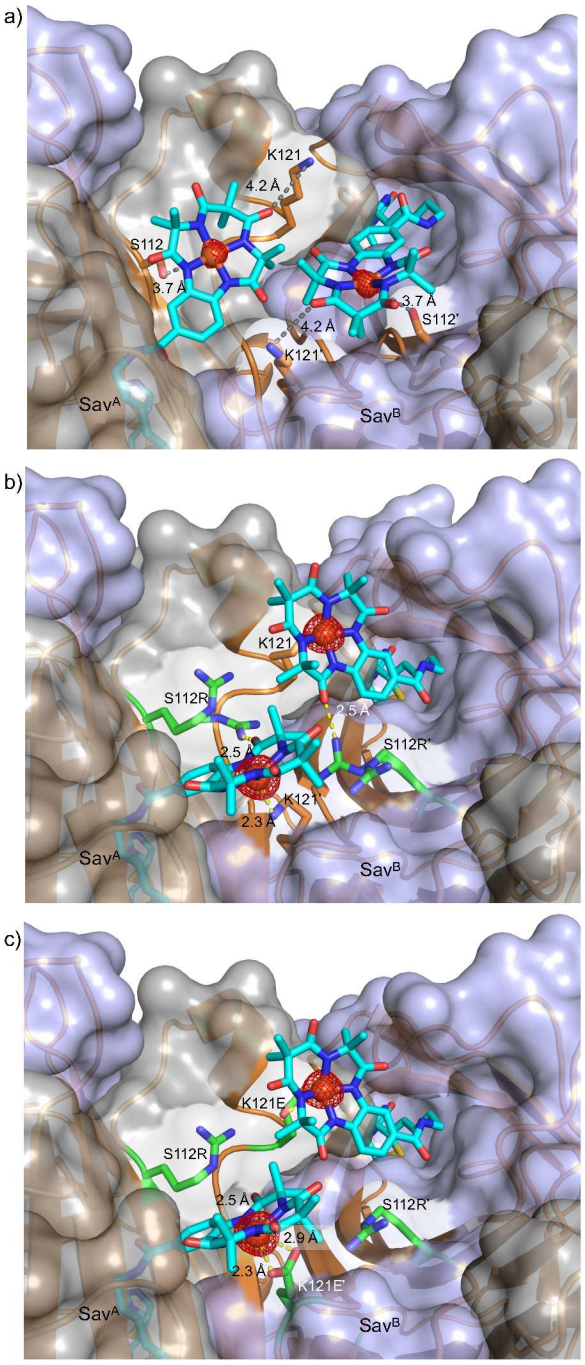

Figure 1. Crystallographic characterization of **biot^{C4}–1**·Sav WT (a, PDB: 6Y2T), **biot^{C4}–1**·Sav S112R (b, PDB: 6Y2M) and **biot^{C4}–1**·Sav S112R/K121E (c, PDB: 6Y25). Sav is depicted as orange cartoon and its surface representation in grey and mauve (for Sav^A and Sav^B monomers respectively). The cofactor and relevant amino acids are depicted as sticks. The Fe atoms are depicted as spheres and surrounded by their anomalous electron density (red mesh at 5 σ).

The oxidation of indane and tetralin (BDE_{C-H} = 87 and 85.7 kcal/mol)[69] afforded high TTON (205 and 316 TTON respectively) and good ee in favor of the (*R*)-alcohol (47% and 65% ee respectively, Table 1).

Table 1. Benzylic C–H oxidations catalyzed by biot^{C4}–1·Sav S112R.[a]

Substrate		TTON	ee (%)	[alcohol]/[ketone]	Conversion (%) (alcohol yield (%))[c]
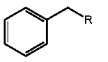	R = CH_3	57	32	3.2	11.5 (8.8)
	R = CH_2CH_3	26	45	8.4	5.9 (5.3)
	R = $(CH_2)_2CH_3$	19	45	7.5	4.3 (3.8)
	R = $C(CH_3)_2$	0	-	-	-
	n = 2	316	65	5.7	60 (44.3)
		300[b]	>98	1.1	86.8 (34.3)
	n = 1	205	47	7.4	45.7 (40.2)
		173[b]	80	0.8	55.7 (24.7)
	n = 0	0	-	-	-
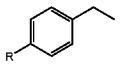	R = OCH_3	120	12	5.9	26.3 (22.5)
	R = Cl	20	14	3.8	4.1 (3.3)
	R = Br	9	18	>20	2.3 (2.3)

[a]Conditions: 25μM **biot^{C4}–1**·Sav S112R (50μM Fe), 20 mM substrate, 20 mM H_2O_2, 50 mM KPB pH 8.5, 35% acetone, 2.5% MeCN, 3 h at 25 ºC. [b]10 mM substrate, 25 mM H_2O_2, to promote alcohol overoxidation which yields increased ee. [c]See Table S6 for more details.

Prompted by the good TTON and ee for tetralin, its oxidation by **biot^{C4}–1**·Sav S112R was scrutinized. Using 2.5 equiv H_2O_2, 73% ee of (*R*)-tetralol was determined at early stages (Scheme 3a). In contrast to PhEt oxidation, the ee increased with conversion, highlighting the preferential (over)oxidation of (*S*)-tetralol. After 3 h, > 98% ee (*R*)-tetralol was obtained (300 TTON, Scheme 3b). Minimal overoxidation at the second benzylic position was also detected (Figure S17). Oxidation of (*rac*)-tetralol with **biot^{C4}–1**·Sav S112R yielded tetralone and > 99% ee of (*R*)-tetralol (unreacted starting material) after ~120 minutes (Scheme 3c, $E = k_{(S)} / k_{(R)} = 2.7$, and S18). Similarly, 173 TTON are obtained for indane oxidation (80% ee (*R*)-indanol, Figure S19). Thus, (*R*)-benzyl-alcohol derivatives are preferentially overoxidized, while the (*S*)-enantiomer of the cyclic derivatives (tetralol and indanol) are oxidized faster. This phenomenon can be attributed to the 1,3-allylic strain (Scheme S2).[70,71]

Lastly, we developed an enzymatic cascade with Glucose Oxidase (GO) to enable the *in-situ* production of H_2O_2, using O_2 as oxidant and glucose as reductant (Scheme 4).[72] To our delight, after combining **biot^{C4}–1**·Sav S112R and GO the oxidation reactions progressed in a similar way compared to the single batch addition of H_2O_2. 50 TTON were obtained for PhEt oxidation, with an initial ee of (*R*)-PhEtOH of 47%, which eroded to 37% after kinetic resolution. For tetralin 170 TTON were obtained, again observing the initial formation of (*R*)-tetralol in 64% ee and posterior kinetic resolution that upgraded it to up to 95%.

Catalysts derived from earth-abundant metals are gaining attention in homogeneous catalysis. The inherent lability of most such systems however limits their use in water. In contrast to polypyridinamine-derived catalysts,[73] and thanks to its remarkable stability and catalytic activity, the Fe(TAML) system proved amenable to the design and optimization of an artificial hydroxylase based on the biotin-streptavidin technology.

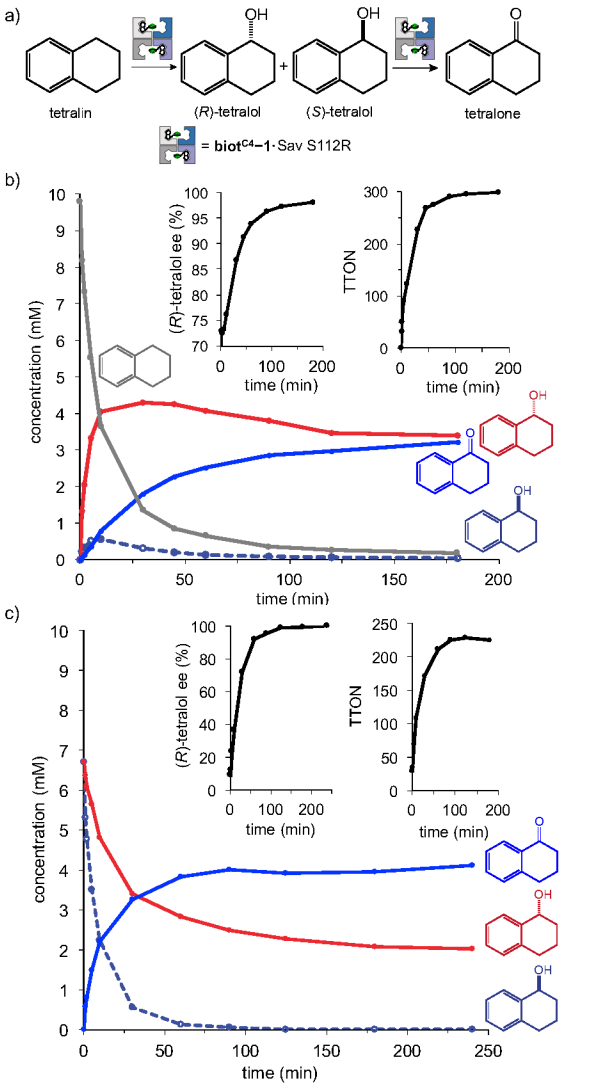

Scheme 3. Enantioselective hydroxylation of tetralin and kinetic resolution of tetralol by **biot^{C4}–1**·Sav S112R a) Consecutive oxidation scheme b) Time course of tetralin oxidation. Inset: kinetic resolution affords > 98% ee (*R*)-tetralol and TTON = 300 c) Time course of the kinetic resolution of *rac*-tetralol by **biot^{C4}–1**·Sav S112R. Inset: kinetic resolution yields > 99% ee (*R*)-tetralol (TTON = 220). See SI for details.

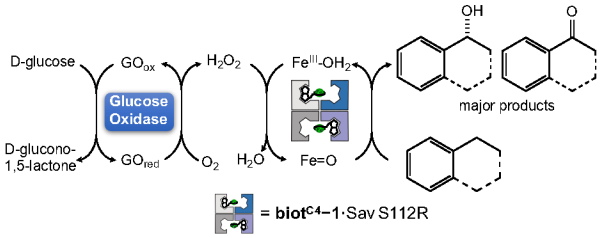

Scheme 4. Cascade with GO to generate H_2O_2 *in situ,* enabling hydroxylation using O_2 as oxidant. See SI.

Chemogenetic optimization of the catalytic performance led to the identification of **biot^{C4}–1**·Sav S112R as our best hydroxylase for the oxidation of benzylic C–H bonds. With

in vivo applications in mind, we have shown that the activity of the artificial hydroxylase is compatible with glucose oxidase, using O_2 as the terminal oxidant.

Efforts at modulating the activity of the hydroxylase by fine-tuning the cofactors' structure, and expanding the substrate scope towards the oxidation of more complex molecules are currently underway.

ASSOCIATED CONTENT

The Supporting Information is available free of charge on the ACS Publications website. General information, experimental section, Figures S1−S21, Tables S1−S6, Scheme S1−S2.

AUTHOR INFORMATION

Corresponding Author

Correspondence should be addressed to thomas.ward@unibas.ch

ORCID

Joan Serrano-Plana 0000-0003-2735-0943
Corentin Rumo 0000-0001-7411-5212
Johannes G. Rebelein: 0000-0003-2560-716X
Ryan L. Peterson: 0000-0002-9654-703X
Thomas R. Ward: 0000-0001-8602-5468

Notes

The authors declare no competing financial interest

ACKNOWLEDGMENTS

TRW thanks the University of Basel, the NCCR Molecular Systems engineering, the SNF (grant 200020_182046) and the ERC (the DrEAM, advanced grant 694424). JS-P thanks the EU for a Marie Skłodowska-Curie fellowship (H2020-MSCA-IF-2016). JGR thanks the European Molecual Biology Organisation for a long-term fellowship (ALTF-194-2017).

REFERENCES

1. Hartwig, J. F.; Larsen, M. A., Undirected, Homogeneous C–H Bond Functionalization: Challenges and Opportunities. *ACS Cent. Sci.* **2016,** *2*, 281-292.
2. Bergman, R. G., C–H activation. *Nature* **2007,** *446*, 391-393.
3. Ye, B.; Zhao, J.; Zhao, K.; McKenna, J. M.; Toste, F. D., Chiral Diaryliodonium Phosphate Enables Light Driven Diastereoselective α-C(sp3)–H Acetalization. *J. Am. Chem. Soc.* **2018,** *140*, 8350-8356.
4. Hartwig, J. F., Evolution of C–H Bond Functionalization from Methane to Methodology. *J. Am. Chem. Soc.* **2016,** *138*, 2-24.
5. Wencel-Delord, J.; Glorius, F., C–H bond activation enables the rapid construction and late-stage diversification of functional molecules. *Nat. Chem.* **2013,** *5*, 369-375.
6. Labinger, J. A.; Bercaw, J. E., Understanding and exploiting C–H bond activation. *Nature* **2002,** *417*, 507-514.
7. Newton, C. G.; Wang, S.-G.; Oliveira, C. C.; Cramer, N., Catalytic Enantioselective Transformations Involving C–H Bond Cleavage by Transition-Metal Complexes. *Chem. Rev.* **2017,** *117*, 8908-8976.
8. Costas, M.; Mehn, M. P.; Jensen, M. P.; Que, L., Dioxygen Activation at Mononuclear Nonheme Iron Active Sites: Enzymes, Models, and Intermediates. *Chem. Rev.* **2004,** *104*, 939-986.
9. Lewis, J. C.; Coelho, P. S.; Arnold, F. H., Enzymatic functionalization of carbon–hydrogen bonds. *Chem. Soc. Rev.* **2011,** *40*, 2003-2021.
10. Ortiz de Montellano, P. R., Hydrocarbon Hydroxylation by Cytochrome P450 Enzymes. *Chem. Rev.* **2010,** *110*, 932-948.
11. Adam, W.; Lukacs, Z.; Harmsen, D.; Saha-Möller, C. R.; Schreier, P., Biocatalytic Asymmetric Hydroxylation of Hydrocarbons with the Topsoil-Microorganism Bacillus megaterium. *J. Org. Chem.* **2000,** *65*, 878-882.
12. Nam, W., Synthetic Mononuclear Nonheme Iron–Oxygen Intermediates. *Acc. Chem. Res.* **2015,** *48*, 2415-2423.
13. Jasniewski, A. J.; Que, L., Dioxygen Activation by Nonheme Diiron Enzymes: Diverse Dioxygen Adducts, High-Valent Intermediates, and Related Model Complexes. *Chem. Rev.* **2018,** *118*, 2554-2592.
14. Que, L.; Tolman, W. B., Biologically inspired oxidation catalysis. *Nature* **2008,** *455*, 333-340.
15. Bruijnincx, P. C. A.; van Koten, G.; Klein Gebbink, R. J. M., Mononuclear non-heme iron enzymes with the 2-His-1-carboxylate facial triad: recent developments in enzymology and modeling studies. *Chem. Soc. Rev.* **2008,** *37*, 2716-2744.
16. Battistella, B.; Ray, K., O2 and H_2O_2 activations at dinuclear Mn and Fe active sites. *Coord. Chem. Rev.* **2020,** *408*, 213176.
17. Ray, K.; Pfaff, F. F.; Wang, B.; Nam, W., Status of Reactive Non-Heme Metal–Oxygen Intermediates in Chemical and Enzymatic Reactions. *J. Am. Chem. Soc.* **2014,** *136*, 13942-13958.
18. Zheng, C.; You, S.-L., Recent development of direct asymmetric functionalization of inert C–H bonds. *RSC Adv.* **2014,** *4*, 6173-6214.
19. Milan, M.; Bietti, M.; Costas, M., Enantioselective aliphatic C–H bond oxidation catalyzed by bioinspired complexes. *Chem. Commun.* **2018,** *54*, 9559-9570.
20. Saint-Denis, T. G.; Zhu, R.-Y.; Chen, G.; Wu, Q.-F.; Yu, J.-Q., Enantioselective C(sp^3)–H bond activation by chiral transition metal catalysts. *Science* **2018,** *359*, eaao4798.
21. White, M. C.; Zhao, J., Aliphatic C–H Oxidations for Late-Stage Functionalization. *J. Am. Chem. Soc.* **2018,** *140*, 13988-14009.
22. Shugrue, C. R.; Miller, S. J., Applications of Nonenzymatic Catalysts to the Alteration of Natural Products. *Chem. Rev.* **2017,** *117*, 11894-11951.
23. Groves, J. T.; Viski, P., Asymmetric hydroxylation by a chiral iron porphyrin. *J. Am. Chem. Soc.* **1989,** *111*, 8537-8538.
24. Frost, J. R.; Huber, S. M.; Breitenlechner, S.; Bannwarth, C.; Bach, T., Enantiotopos-Selective C-H Oxygenation Catalyzed by a Supramolecular Ruthenium Complex. *Angew. Chem. Int. Ed.* **2015,** *54*, 691-695.
25. Burg, F.; Gicquel, M.; Breitenlechner, S.; Pöthig, A.; Bach, T., Site- and Enantioselective C−H Oxygenation Catalyzed by a Chiral Manganese Porphyrin Complex with a Remote Binding Site. *Angew. Chem. Int. Ed.* **2018,** *57*, 2953-2957.
26. Murahashi, S.-I.; Noji, S.; Komiya, N., Catalytic Enantioselective Oxidation of Alkanes and Alkenes Using (Salen)Manganese Complexes Bearing a Chiral Binaphthyl Strapping Unit. *Adv. Synth. Catal.* **2004,** *346*, 195-198.
27. Srour, H.; Maux, P. L.; Simonneaux, G., Enantioselective Manganese-Porphyrin-Catalyzed Epoxidation and C–H Hydroxylation with Hydrogen Peroxide in Water/Methanol Solutions. *Inorg. Chem.* **2012,** *51*, 5850-5856.
28. Komiya, N.; Noji, S.; Murahashi, S.-I., Manganese catalyzed asymmetric oxidation of alkanes to optically active ketones bearing asymmetric center at the α-position. *Tetrahedron Lett.* **1998,** *39*, 7921-7924.
29. Milan, M.; Bietti, M.; Costas, M., Highly Enantioselective Oxidation of Nonactivated Aliphatic C–H Bonds with Hydrogen Peroxide Catalyzed by Manganese Complexes. *ACS Cent. Sci.* **2017,** *3*, 196-204.
30. Hamada, T.; Irie, R.; Mihara, J.; Hamachi, K.; Katsuki, T., Highly enantioselective benzylic hydroxylation with concave type of (salen)manganese(III) complex. *Tetrahedron* **1998,** *54*, 10017-10028.
31. Olivo, G.; Farinelli, G.; Barbieri, A.; Lanzalunga, O.; Di Stefano, S.; Costas, M., Supramolecular Recognition Allows Remote, Site-Selective C−H Oxidation of Methylenic Sites in Linear Amines. *Angew. Chem. Int. Ed.* **2017,** *56*, 16347-16351.
32. Gormisky, P. E.; White, M. C., Catalyst-Controlled Aliphatic C–H Oxidations with a Predictive Model for Site-Selectivity. *J. Am. Chem. Soc.* **2013,** *135*, 14052-14055.

33. Chen, M. S.; White, M. C., A Predictably Selective Aliphatic C–H Oxidation Reaction for Complex Molecule Synthesis. *Science* **2007,** *318*, 783-787.
34. Schwizer, F.; Okamoto, Y.; Heinisch, T.; Gu, Y.; Pellizzoni, M. M.; Lebrun, V.; Reuter, R.; Köhler, V.; Lewis, J. C.; Ward, T. R., Artificial Metalloenzymes: Reaction Scope and Optimization Strategies. *Chem. Rev.* **2018,** *118*, 142-231.
35. Pàmies, O.; Diéguez, M.; Bäckvall, J.-E., Artificial Metalloenzymes in Asymmetric Catalysis: Key Developments and Future Directions. *Adv. Synth. Catal.* **2015,** *357*, 1567-1586.
36. Upp, D. M.; Lewis, J. C., Selective C–H bond functionalization using repurposed or artificial metalloenzymes. *Curr. Opin. Chem. Biol.* **2017,** *37*, 48-55.
37. Perez-Rizquez, C.; Rodriguez-Otero, A.; Palomo, J. M., Combining enzymes and organometallic complexes: novel artificial metalloenzymes and hybrid systems for C–H activation chemistry. *Org. Biomol. Chem.* **2019,** *17*, 7114-7123.
38. Davis, H. J.; Ward, T. R., Artificial Metalloenzymes: Challenges and Opportunities. *ACS Cent. Sci.* **2019,** *5*, 1120-1136.
39. Lewis, J. C., Artificial Metalloenzymes and Metallopeptide Catalysts for Organic Synthesis. *ACS Catal.* **2013,** *3*, 2954-2975.
40. Monnard, F. W.; Nogueira, E. S.; Heinisch, T.; Schirmer, T.; Ward, T. R., Human carbonic anhydrase II as host protein for the creation of artificial metalloenzymes: the asymmetric transfer hydrogenation of imines. *Chem. Sci.* **2013,** *4*, 3269-3274.
41. Oohora, K.; Onoda, A.; Hayashi, T., Hemoproteins Reconstituted with Artificial Metal Complexes as Biohybrid Catalysts. *Acc. Chem. Res.* **2019,** *52*, 945-954.
42. Mirts, E. N.; Petrik, I. D.; Hosseinzadeh, P.; Nilges, M. J.; Lu, Y., A designed heme-[4Fe-4S] metalloenzyme catalyzes sulfite reduction like the native enzyme. *Science* **2018,** *361*, 1098-1101.
43. Lewis, J. C., Beyond the Second Coordination Sphere: Engineering Dirhodium Artificial Metalloenzymes To Enable Protein Control of Transition Metal Catalysis. *Acc. Chem. Res.* **2019,** *52*, 576-584.
44. Roelfes, G., LmrR: A Privileged Scaffold for Artificial Metalloenzymes. *Acc. Chem. Res.* **2019,** *52*, 545-556.
45. Chino, M.; Maglio, O.; Nastri, F.; Pavone, V.; DeGrado, W. F.; Lombardi, A., Artificial Diiron Enzymes with a De Novo Designed Four-Helix Bundle Structure. *Eur. J. Inorg. Chem.* **2015,** *2015*, 3371-3390.
46. Lombardi, A.; Pirro, F.; Maglio, O.; Chino, M.; DeGrado, W. F., De Novo Design of Four-Helix Bundle Metalloproteins: One Scaffold, Diverse Reactivities. *Acc. Chem. Res.* **2019,** *52*, 1148-1159.
47. Grimm, A. R.; Sauer, D. F.; Polen, T.; Zhu, L.; Hayashi, T.; Okuda, J.; Schwaneberg, U., A Whole Cell E. Coli Display Platform for Artificial Metalloenzymes: Poly(phenylacetylene) Production with a Rhodium–Nitrobindin Metalloprotein. *ACS Catal.* **2018,** *8*, 2611-2614.
48. Heinisch, T.; Ward, T. R., Artificial Metalloenzymes Based on the Biotin–Streptavidin Technology: Challenges and Opportunities. *Acc. Chem. Res.* **2016,** *49*, 1711-1721.
49. Liang, A. D.; Serrano-Plana, J.; Peterson, R. L.; Ward, T. R., Artificial Metalloenzymes Based on the Biotin–Streptavidin Technology: Enzymatic Cascades and Directed Evolution. *Acc. Chem. Res.* **2019,** *52*, 585-595.
50. Wilson, M. E.; Whitesides, G. M., Conversion of a protein to a homogeneous asymmetric hydrogenation catalyst by site-specific modification with a diphosphinerhodium(I) moiety. *J. Am. Chem. Soc.* **1978,** *100*, 306-307.
51. Oohora, K.; Kihira, Y.; Mizohata, E.; Inoue, T.; Hayashi, T., C(sp3)–H Bond Hydroxylation Catalyzed by Myoglobin Reconstituted with Manganese Porphycene. *J. Am. Chem. Soc.* **2013,** *135*, 17282-17285.
52. Kille, S.; Zilly, F. E.; Acevedo, J. P.; Reetz, M. T., Regio- and stereoselectivity of P450-catalysed hydroxylation of steroids controlled by laboratory evolution. *Nat. Chem.* **2011,** *3*, 738-743.
53. Zhang, K.; Shafer, B. M.; Demars, M. D.; Stern, H. A.; Fasan, R., Controlled Oxidation of Remote sp3 C–H Bonds in Artemisinin via P450 Catalysts with Fine-Tuned Regio- and Stereoselectivity. *J. Am. Chem. Soc.* **2012,** *134*, 18695-18704.
54. Peters, M. W.; Meinhold, P.; Glieder, A.; Arnold, F. H., Regio- and Enantioselective Alkane Hydroxylation with Engineered Cytochromes P450 BM-3. *J. Am. Chem. Soc.* **2003,** *125*, 13442-13450.
55. Collins, T. J., TAML Oxidant Activators: A New Approach to the Activation of Hydrogen Peroxide for Environmentally Significant Problems. *Acc. Chem. Res.* **2002,** *35*, 782-790.
56. Collins, T. J.; Ryabov, A. D., Targeting of High-Valent Iron-TAML Activators at Hydrocarbons and Beyond. *Chem. Rev.* **2017,** *117*, 9140-9162.
57. Chahbane, N.; Popescu, D.-L.; Mitchell, D. A.; Chanda, A.; Lenoir, D.; Ryabov, A. D.; Schramm, K.-W.; Collins, T. J., FeIII–TAML-catalyzed green oxidative degradation of the azo dye Orange II by H2O2 and organic peroxides: products, toxicity, kinetics, and mechanisms. *Green Chem.* **2007,** *9*, 49-57.
58. Ryabov, A. D.; Collins, T. J., Mechanistic considerations on the reactivity of green Fe^{III}-TAML activators of peroxides. *Adv. Inorg. Chem.* **2009,** *61*, 471-521.
59. Ghosh, M.; Nikhil, Y. L. K.; Dhar, B. B.; Sen Gupta, S., Mechanism of Alcohol Oxidation by Fe^{V}(O) at Room Temperature. *Inorg. Chem.* **2015,** *54*, 11792-11798.
60. Kwon, E.; Cho, K.-B.; Hong, S.; Nam, W., Mechanistic insight into the hydroxylation of alkanes by a nonheme iron(v)–oxo complex. *Chem. Commun.* **2014,** *50*, 5572-5575.
61. Napoly, F.; Kieffer, R.; Jean-Gérard, L.; Goux-Henry, C.; Draye, M.; Andrioletti, B., Fe(TAML)Li/tert-butyl hydroperoxide as a new combination for benzylic C–H oxidation. *Tetrahedron Lett.* **2015,** *56*, 2517-2520.
62. Das, A.; Nutting, J. E.; Stahl, S. S., Electrochemical C–H oxygenation and alcohol dehydrogenation involving Fe-oxo species using water as the oxygen source. *Chem. Sci.* **2019,** *10*, 7542-7548.
63. Dundas, C. M.; Demonte, D.; Park, S., Streptavidin–biotin technology: improvements and innovations in chemical and biological applications. *Appl. Microbiol. Biotechnol.* **2013,** *97*, 9343-9353.
64. Ren, Q.; Guo, Y.; Mills, M. R.; Ryabov, A. D.; Collins, T. J., On the Iron(V) Reactivity of an Aggressive Tail-Fluorinated Tetraamido Macrocyclic Ligand (TAML) Activator. *Eur. J. Inorg. Chem.* **2015,** *2015*, 1445-1452.
65. acetone was selected as co-solvent to ensure dissolution of the substrates. Its presence influences the product distribution by diminishing alcohol oxidation. See SI for more details.
66. TTON refers to total turnover number, and includes the C-H hydroxylation and alcohol oxidation products, quantified by GC-FID. See SI for more details.
67. Ghosh, M.; Singh, K. K.; Panda, C.; Weitz, A.; Hendrich, M. P.; Collins, T. J.; Dhar, B. B.; Sen Gupta, S., Formation of a Room Temperature Stable Fe^{V}(O) Complex: Reactivity Toward Unactivated C–H Bonds. *J. Am. Chem. Soc.* **2014,** *136*, 9524-9527.
68. Kundu, S.; Thompson, J. V. K.; Shen, L. Q.; Mills, M. R.; Bominaar, E. L.; Ryabov, A. D.; Collins, T. J., Activation Parameters as Mechanistic Probes in the TAML Iron(V)–Oxo Oxidations of Hydrocarbons. *Chem. Eur. J.* **2015,** *21*, 1803-1810.
69. St. John, P. C.; Guan, Y.; Kim, Y.; Kim, S.; Paton, R. S. Prediction of organic homolytic bond dissociation enthalpies at near chemical accuracy with sub-second computational cost. *Nat. Commun.* **2020**, 11, 2328.
70. Hoffmann, R. W., Allylic 1,3-strain as a controlling factor in stereoselective transformations. *Chem. Rev.* **1989,** *89*, 1841-1860.
71. Shin-ya, K.; Sugeta, H.; Shin, S.; Hamada, Y.; Katsumoto, Y.; Ohno, K., Absolute Configuration and Conformation Analysis of 1-Phenylethanol by Matrix-Isolation Infrared and Vibrational Circular Dichroism Spectroscopy Combined with Density Functional Theory Calculation. *J. Phys. Chem. A* **2007,** *111*, 8598-8605.
72. Miller, J. A.; Alexander, L.; Mori, D. I.; Ryabov, A. D.; Collins, T. J., In situ enzymatic generation of H_2O_2 from O_2 for use in oxidative bleaching and catalysis by TAML activators. *New J. Chem.* **2013,** *37*, 3488-3495.
73. Doble, M. V.; Jarvis, A. G.; Ward, A. C. C.; Colburn, J. D.; Götze, J. P.; Bühl, M.; Kamer, P. C. J., Artificial Metalloenzymes as Catalysts for Oxidative Lignin Degradation. *ACS Sustain. Chem. Eng.* **2018,** *6*, 15100-15107.

Insert Table of Contents artwork here